

Dust in Active Galactic Nuclei

Aigen Li

*Department of Physics and Astronomy, University of Missouri,
Columbia, MO 65211, USA; email: lia@missouri.edu*

Abstract. Dust plays an essential role in the unification theory of active galactic nuclei (AGNs). This review summarizes our current understanding of the extinction and infrared emission properties of the circumnuclear dust in AGNs as well as the inferred dust composition and size distribution.

1. Introduction: Are All AGNs Born Equal? — The Role of Dust in the Unified Schemes of AGNs

Dust is the cornerstone of the unification theory of active galactic nuclei (AGNs). This theory proposes that all AGNs are essentially “born equal”: all types of AGNs are surrounded by an optically thick dust torus and are basically the same object but viewed from different lines of sight (see e.g. Antonucci 1993; Urry & Padovani 1995). The large diversity in the observational properties of AGNs (e.g. optical emission-line widths and X-ray spectral slopes) is simply caused by the viewing-angle-dependent obscuration of the nucleus: those viewed face-on are unobscured (allowing for a direct view of their nuclei) and recognized as “type 1” AGNs, while those viewed edge-on are “type 2” AGNs with most of their central engine and broad line regions being hidden by the obscuring dust.

Apparently, key factors in understanding the structure and nature of AGNs are determining the geometry of the nuclear obscuring torus around the central engine and the obscuration (i.e. extinction, a combination of absorption and scattering) properties of the circumnuclear dust. An accurate knowledge of the dust extinction properties is also required to correct for the dust obscuration in order to recover the intrinsic optical/ultraviolet (UV) spectrum of the nucleus from the observed spectrum and to probe the physical conditions of the dust-enshrouded gas close to the nucleus.

The presence of an obscuring dust torus around the central engine was first indirectly indicated by the spectropolarimetric detection of broad permitted emission lines (characteristic of type 1 AGNs) scattered into our line of sight by free electrons located above or below the dust torus in a number of type 2 AGNs (e.g. see Heisler et al. 1997, Tran 2003). Direct evidence for the presence of a dust torus is provided by infrared (IR) observations. The circumnuclear dust absorbs the AGN illumination and reradiates the absorbed energy in the IR. The IR emission at wavelengths longward of $\lambda > 1 \mu\text{m}$ accounts for at least 50% of the bolometric luminosity of type 2 AGNs. For type 1 AGNs, $\sim 10\%$ of the bolometric luminosity is emitted in the IR (e.g. see Fig. 13.7 of Osterbrock & Ferland 2006). A near-IR “bump” (excess emission above the $\sim 2\text{--}10 \mu\text{m}$ continuum), generally attributed to hot dust with temperatures around $\sim 1200\text{--}1500 \text{ K}$ (near the sublimation temperatures of silicate and graphite grains), is seen in a few type 1 AGNs (Barvainis 1987; Rodríguez-Ardila & Mazzalay 2006). Direct imaging at near- and mid-IR wavelengths has been performed for several

AGNs and provides constraints on the size and structure of the circumnuclear dust torus (e.g. see Jaffe et al. 2004, Elitzur 2006). Spectroscopically, the $10\ \mu\text{m}$ silicate *absorption* feature (see §3.3) and the $3.4\ \mu\text{m}$ aliphatic hydrocarbon *absorption* feature (see §3.2) are widely seen in heavily obscured type 2 AGNs; in contrast, the $10\ \mu\text{m}$ silicate *emission* feature has recently been detected in a number of type 1 AGNs (see §3.3).

To properly interpret the observed IR continuum emission and spectroscopy as well as the IR images of AGNs, it requires a good understanding of the absorption and emission properties of the circumnuclear dust. To this end, one needs to know the composition, size, and morphology of the dust – with this knowledge, one can use Mie theory (for spherical dust) to calculate the absorption and scattering cross sections of the dust from X-ray to far-IR wavelengths, and then calculate its UV/optical/near-IR obscuration as a function of wavelength, and derive the dust thermal equilibrium temperature (based on the energy balance between absorption and emission) as well as its IR emission spectrum. This will allow us to correct for dust obscuration and constrain the circumnuclear structure through modeling the observed IR emission and images. The former is essential for interpreting the obscured UV/optical emission lines and probing the physical conditions of the central regions; the latter is critical to our understanding of the growth of the central supermassive black hole.

However, little is known about the dust in the circumnuclear torus of AGNs. Even our knowledge of the best-studied dust – the Milky Way interstellar dust – is very limited. In this review, I will take a comparative study of the extinction and IR emission as well as the UV/IR spectroscopic properties and the inferred composition, size and morphology of the dust in AGNs and the dust in the interstellar medium (ISM) of the Milky Way and other galaxies.

2. Extinction — A Powerful Discriminator of Dust Size

Extinction is a combined effect of absorption and scattering. Since a grain absorbs and scatters light most effectively at wavelengths comparable to its size $\lambda \approx 2\pi a$, the wavelength dependence of extinction (“extinction curve”) constrains the dust size distribution.

2.1. Interstellar Extinction: Milky Way, SMC, and LMC

Interstellar extinction is most commonly obtained through the “pair-method” by comparing the spectra of two stars of the same spectral type, one of which is reddened and the other unreddened. Interstellar extinction curves rise from the near-IR to the near-UV, with a broad absorption feature at about $\lambda^{-1} \approx 4.6\ \mu\text{m}^{-1}$ ($\lambda \approx 2175\ \text{\AA}$), followed by a steep rise into the far-UV $\lambda^{-1} \approx 10\ \mu\text{m}^{-1}$ (see Fig. 1). This wavelength dependence indicates that there must exist in the ISM a population of large grains with $a \gtrsim \lambda/2\pi \approx 0.1\ \mu\text{m}$ to account for the extinction at visible/near-IR wavelengths, and a population of ultrasmall grains with $a \lesssim \lambda/2\pi \approx 0.016\ \mu\text{m}$ to account for the far-UV extinction at $\lambda = 0.1\ \mu\text{m}$. In the wavelength range of $0.125 \leq \lambda \leq 3.5\ \mu\text{m}$, the Galactic extinction curves can be approximated by an analytical formula involving only one free parameter: $R_V \equiv A_V/E(B - V)$, the total-to-selective extinction ratio (Cardelli et al. 1989), with $R_V \approx 3.1$ for the Galactic average (see Fig. 1). The optical/UV extinction curves and R_V show considerable regional variations and depend on the environment: lower-density regions have a smaller R_V , a stronger 2175 Å bump and a steeper far-UV rise

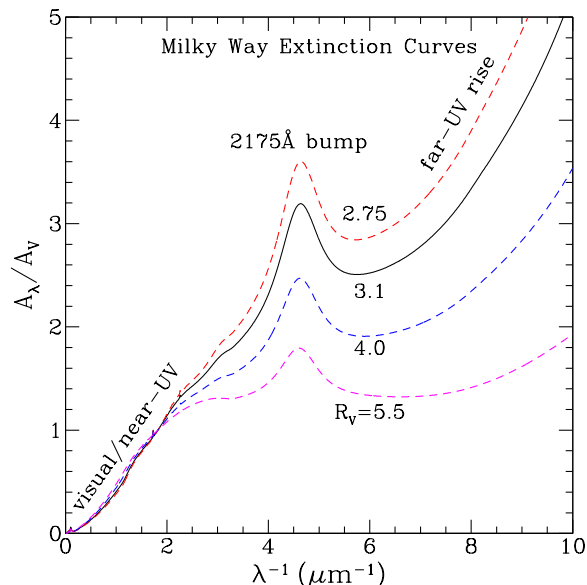


Figure 1. Interstellar extinction curves of the Milky Way ($R_V = 2.75, 3.1, 4.0, 5.5$). There exist considerable regional variations in the Galactic optical/UV extinction curves, as characterized by the total-to-selective extinction ratio R_V , indicating that dust grains on different sightlines have different size distributions.

($\lambda^{-1} > 4 \mu\text{m}^{-1}$), implying smaller dust in these regions; denser regions have a larger R_V , a weaker 2175 Å bump and a flatter far-UV rise, implying larger dust.

In the Small Magellanic Cloud (SMC), the extinction curves of most sightlines display a nearly linear steep rise with λ^{-1} and an extremely weak or absent 2175 Å bump (Lequeux et al. 1982; Prévot et al. 1984; see Fig. 2), suggesting that the dust in the SMC is smaller than that in the Galactic diffuse ISM as a result of either more efficient dust destruction in the SMC due to its harsh environment of the copious star formation associated with the SMC Bar or lack of growth due to the low-metallicity of the SMC, or both. The Large Magellanic Cloud (LMC) extinction curve is characterized by a weaker 2175 Å bump and a stronger far-UV rise than the Galactic curve (Nandy et al. 1981; Koornneef & Code 1981), intermediate between that of the SMC and that of the Galaxy (see Fig. 2). Regional variations also exist in the SMC and LMC extinction curves.

2.2. AGN Extinction — “Gray” or SMC-like Extinction?

Little is known about the wavelength dependence of the extinction caused by the circumnuclear dust of AGNs. In literature, the AGN extinction curves are mainly inferred from (1) composite quasar spectra, and (2) individual reddened AGNs. The former often reveals a “gray” extinction, implying that the size distribution of the dust in the AGN circumnuclear environments is skewed towards substantially large grains. The latter often suggests a steep-rising SMC-like extinction, indicating a preponderance of small grains near the nucleus. There is also indirect information, including the dust reddening- and extinction-to-gas ratios and the IR emission modeling of AGNs (see §4).

Composite Reddened Quasar Spectra — “Gray” Extinction? Czerny et al. (2004) constructed a quasar extinction curve based on the blue and red composite

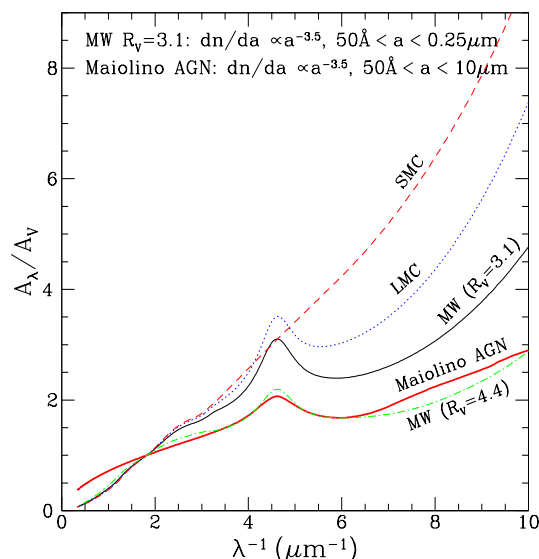


Figure 2. Interstellar extinction curves of the Milky Way ($R_V = 3.1$, 4.4), SMC, and LMC. Also plotted is the “Maiolino”-type extinction curve for AGNs (similar to the Galactic $R_V = 4.4$ curve) produced by a mixture of interstellar silicate and graphite grains with a size distribution of $dn/da \sim a^{-3.5}$ ($50 \text{ \AA} < a < 10 \mu\text{m}$), the same as that for the Galactic average $R_V = 3.1$ except with a smaller upper cutoff for the latter ($50 \text{ \AA} < a < 0.25 \mu\text{m}$).

quasar spectra of Richards et al. (2003) obtained from the Sloan Digital Sky Survey (SDSS). Six composite quasar spectra were generated by Richards et al. (2003) from 4576 SDSS quasars based on the relative $g^* - i^*$ color with “Composite 1” (made from 770 objects) being the bluest. Czerny et al. (2004) created a mean “quasar extinction curve” by averaging 3 extinction curves obtained through comparing the spectra of Composites 3, 4, and 5 (consisting of 770, 770, and 211 objects, respectively) with that of Composite 1, assuming that Composite 1 is essentially unaffected by dust while Composites 3, 4, and 5 are subject to dust reddening. The resulting extinction curve is nearly monotonic with wavelength, without any trace of the 2175 Å bump (see Fig. 3).

Gaskell et al. (2004) derived extinction curves for radio-loud quasars based on the composite spectra of 72 radio quasars created by Baker & Hunstead (1995), and for radio-quiet AGNs based on the composite spectrum of 1018 radio-quiet AGNs generated by Francis et al. (1991). The extinction curve for these radio-loud quasars, grouped by Baker & Hunstead (1995) into 4 subsamples according to the 5 GHz radio core-to-lobe flux ratios R , was determined by comparing the composite spectrum of the more-reddened lobe-dominant ($R < 0.1$) sample with that of less-reddened core-dominant ($R > 1$) sample. Similarly, Gaskell et al. (2004) obtained an extinction curve for radio-quiet AGNs by comparing the composite spectrum of Francis et al. (1991) created for 1018 radio-quiet AGNs with that for the relatively unreddened core-dominant composite of Baker & Hunstead (1995). Most prominently, the derived extinction curves for both radio-loud quasars and radio-quiet quasars lack the 2175 Å bump and are essentially “gray”, i.e., significantly flatter in the UV than that of the Milky

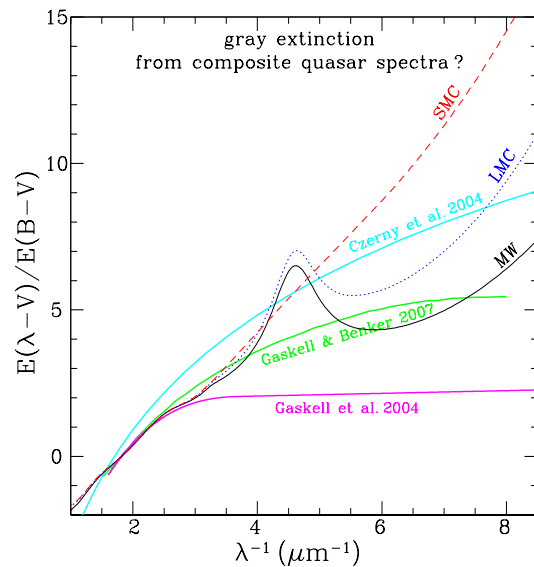


Figure 3. Comparison of the AGN extinction curves derived from composite quasar spectra (Czerny et al. 2004, Gaskell et al. 2004) with that for the Milky Way, SMC, and LMC. For comparison, also shown is the average extinction curve obtained for individual AGNs by Gaskell & Benker (2007).

Way diffuse ISM, although it appears that for the latter the reddening curve is slightly steeper in the UV (see Fig. 3).

However, Willott (2005) questioned the validity of the approach based on the ratios of reddened and unreddened composite quasars (Czerny et al. 2004; Gaskell et al. 2004) since composite spectra combine quasars at different redshifts, while the quasars going into a composite spectrum have a negative correlation between reddening and redshift, and quasar surveys in practice contain more highly reddened quasars at lower redshifts. He argued that since the quasars contributing to the composite in the UV have typically lower reddening than those contributing in the optical, the gray UV extinction laws derived using composite quasars (Czerny et al. 2004; Gaskell et al. 2004) might be artificial, and the actual AGN extinction curve may be SMC-like.

Individual Reddened AGNs — SMC-like Extinction? In contrast to the “composite quasar spectrum” method which may be biased by the fact that the highest redshift quasars (which contribute to the UV part of a composite spectrum) are less extinguished (leading to shallower extinction in the UV), AGN extinction curves have also been derived for individual reddened objects.

Crenshaw et al. (2001) determined a reddening curve for the nucleus of the Seyfert 1 galaxy NGC 3227 by comparing its HST/STIS UV and optical spectra with that of the unreddened Seyfert galaxy NGC 4151. They found that the derived extinction curve in the UV is even steeper than that of the SMC and lacks the 2175 Å bump. Similar studies were performed for Ark 564, a Narrow-Line Seyfert 1 galaxy (Crenshaw et al. 2002). By comparing the HST/STIS UV and optical spectra of Ark 564 with that of Mrk 493, an unreddened Narrow-Line Seyfert 1 galaxy, Crenshaw et al. (2002) found that the extinction curve for Ark 564, with no evidence for the 2175 Å bump, rises to the UV more steeply

than the Galactic extinction curve (but not as steeply as the SMC curve) with a longer turning-up wavelength of $\sim 4000 \text{ \AA}$ (compared to $\sim 2500 \text{ \AA}$ for the standard Galactic, LMC, and SMC curves).

In an analysis of the optical/UV color distribution of 4576 SDSS quasars, Richards et al. (2003) showed that 273 (6.0%) of the quasars in their sample appear to be redder because of SMC-like dust extinction and reddening. Hopkins et al. (2004) investigated the reddening law toward 9566 SDSS quasars, including a subset of 1886 quasars matched to 2MASS (Two Micron All Sky Survey) by exploring the shapes of their spectral energy distributions obtained from broadband photometry (at five SDSS bands *ugriz* and three 2MASS bands *JHK*). They found that the reddening toward quasars is dominated by SMC-like dust at the quasar redshift.

More recently, Gaskell & Benker (2007) determined the extinction curves for 14 individual AGNs based on the FUSE and HST spectrophotometry of Shang et al. (2005). Unlike Crenshaw et al. (2001, 2002) who used a single unreddened AGN as a reference, Gaskell & Benker (2007) took the average of 3 AGNs which have the highest $4\text{--}8 \mu\text{m}^{-1}$ fluxes relative to their optical fluxes in the sample of Shang et al. (2005). They found that the majority of the derived extinction curves in the UV are much flatter than that of the SMC, although not as flat as the “gray” curve derived by Gaskell et al. (2004) based on composite quasar spectra (see Fig. 3 for the average extinction curve for the 5 AGNs with the greatest reddening in their sample).

Reduced Reddening- and Extinction-to-Gas Ratios — Flat Extinction? Assuming a Galactic standard extinction curve ($R_V = 3.1$) and a foreground screen, Maiolino et al. (2001a) determined for 19 AGNs the amount of reddening $E(B - V)$ affecting the broad line region by comparing the observed optical/IR H broad line ratios with the intrinsic values. For these AGNs, they also determined the X-ray absorbing column densities N_H from the photoelectric cutoff in their X-ray spectra. They found that for most (16 of 19) objects $E(B - V)/N_H$ is significantly lower than the Galactic standard value ($\approx 1.7 \times 10^{-22} \text{ mag cm}^{-2}$) by a factor ranging from a few to ~ 100 (except for 3 Low Luminosity AGNs whose physics may be intrinsically different [see Ho 1999]). Similarly, Maiolino et al. (2001a) also found that the extinction-to-gas ratios A_V/N_H of various classes of AGNs are significantly lower than the Galactic standard value ($\approx 5.3 \times 10^{-22} \text{ mag cm}^{-2}$). Maiolino et al. (2001b) ascribed the reduced $E(B - V)/N_H$ and A_V/N_H ratios of AGNs (often with a solar or higher metallicity) to grain growth through coagulation in the dense circumnuclear region which results in a dust size distribution biased in favour of large grains and therefore a flat extinction curve.

However, Weingartner & Murray (2002) argued that the X-ray absorption and optical extinction may occur in distinct media (e.g. the X-ray absorption occurs in material located off the torus and/or accretion disk, while the optical extinction occurs in material located beyond the torus); therefore, the reduced $E(B - V)/N_H$ and A_V/N_H ratios may not necessarily imply that the grains in AGNs are systematically larger than those in the Galactic ISM.

3. Dust Spectroscopy — Diagnosis of Dust Composition

Dust spectroscopy provides the most diagnostic information on the dust composition. Our knowledge about the composition of the dust in the Galactic diffuse ISM is mainly derived from the absorption and emission spectral lines:

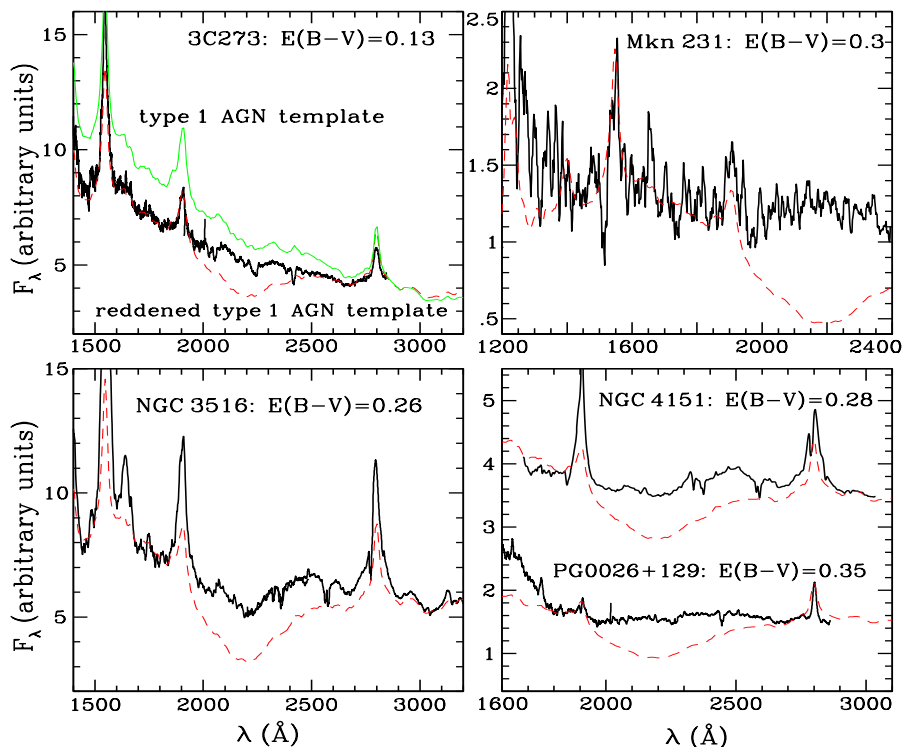


Figure 4. Comparison of the UV spectra (solid lines) of 5 type 1 AGNs (whose broad line ratios and continuum suggest dust absorption) with the template of type 1 AGNs reddened by a standard Galactic extinction ($R_V = 3.1$) with a total amount of reddening $E(B - V)$ consistent with that inferred from the broad lines and adapted to match the shape of the continuum in those regions not affected by the 2175 Å bump (dashed line). Taken from Maiolino et al. (2001a) with modifications.

the 2175 Å extinction bump (small graphitic dust), the 3.4 μm absorption feature (aliphatic hydrocarbon dust), the 9.7 μm and 18 μm absorption features (amorphous silicate dust), and the 3.3, 6.2, 7.7, 8.6, and 11.3 μm emission features (polycyclic aromatic hydrocarbon [PAH] molecules). The ice absorption features at 3.1 and 6.0 μm (H₂O), 4.67 μm (CO), 4.27 and 15.2 μm (CO₂), 3.54 and 9.75 μm (CH₃OH), 2.97 μm (NH₃), 7.68 μm (CH₄), 5.81 μm (H₂CO), and 4.62 μm (XCN⁻) are seen in dark molecular clouds with visual extinction $A_V > 3$ mag. In this section I will present a comparative overview of the dust absorption and emission features in AGNs and the inferred dust composition.

3.1. The 2175 Å Extinction Bump

The 2175 Å extinction bump, first detected over 40 years ago (Stecher 1965), is an ubiquitous feature of the Milky Way ISM. With a stable central wavelength and variable feature strength for lines of sight in our Galaxy, the 2175 Å bump is relatively weaker in the LMC and absent in the SMC (see Fig. 2). This bump is largely absent in AGNs (see §2) except Gaskell & Benker (2007) recently claimed that it might be detected in Mrk 304, one of the seven AGNs with the highest quality extinction curves in their 14-AGN sample. Fig. 4 compares the UV spectra of 5 slightly reddened type 1 AGNs with the template of type 1 AGNs reddened with the standard Galactic extinction. It is seen that the Galactic extinction predicts too strong a 2175 Å dip (Maiolino et al. 2001b).

The exact nature of the 2175 Å bump, the strongest spectroscopic extinction feature in the Galactic ISM, remains uncertain. It is generally believed to be caused by aromatic carbonaceous (graphitic) materials, very likely a cosmic mixture of PAH molecules (Joblin et al. 1992; Li & Draine 2001b). The fact that the 2175 Å bump is not (or at least rarely) seen in AGNs suggests that its carrier (e.g. PAHs) may have been photodestroyed by energetic photons (e.g. X-ray irradiation) from the central engine.

3.2. The 3.4 μm Aliphatic Hydrocarbon Absorption Feature

The 3.4 μm absorption feature, attributed to the C–H stretching mode in saturated aliphatic hydrocarbon dust, is widely seen in the Galactic diffuse ISM (but never seen in molecular clouds; see Pendleton & Allamandola 2002). This feature is also seen in AGNs (Wright et al. 1996, Imanishi et al. 1997, Mason et al. 2004), closely resembling that of our Galaxy in both peak wavelengths and relative feature strengths of the 3.42 μm, 3.48 μm, and 3.51 μm subfeatures (corresponding to symmetric and asymmetric stretches of C–H bonds in CH₂ and CH₃ groups in aliphatic hydrocarbon chains). Mason et al. (2004) argued that the 3.4 μm absorption feature at least in face-on Seyfert 2 galaxies arises in dust local to the active nucleus rather than in the diffuse ISM of the galaxy.

The exact carrier of this feature remains uncertain. So far, among the > 20 candidate materials proposed over the years since its first detection in the Galactic center sightlines 28 years ago, the experimental spectra of hydrogenated amorphous carbon (Mennella et al. 1999) and the organic refractory residue, synthesized from UV photoprocessing of interstellar ice mixtures (Greenberg et al. 1995), provide the best fit to the observed spectra.

So far, no polarization has been detected for this feature (Adamson et al. 1999, Chiar et al. 2006, Mason et al. 2006), suggesting that the carrier of this feature is either spherical or unaligned or both. Spectropolarimetric measurements for both the 9.7 μm silicate and the 3.4 μm hydrocarbon features for the same sightline (e.g. Chiar et al. 2006) would allow for a direct test of the silicate core-hydrocarbon mantle interstellar dust model (Li & Greenberg 1997, Jones et al. 1990), since this model predicts that the 3.4 μm feature would be polarized if the 9.7 μm feature (for the same sightline) is polarized (Li & Greenberg 2002).

3.3. The 9.7 μm and 18 μm Silicate Absorption and Emission Features

The strongest IR absorption features in the Galactic ISM are the 9.7 μm and 18 μm bands, which are almost certainly due to silicate minerals: they are respectively ascribed to the Si–O stretching and O–Si–O bending modes in some form of silicate material (e.g. olivine Mg_{2x}Fe_{2–2x}SiO₄). The observed interstellar silicate bands are broad and relatively featureless, indicating that interstellar silicates are largely amorphous rather than crystalline (Li & Draine [2001a] estimated that the amount of $a < 1$ μm crystalline silicate grains in the Galactic diffuse ISM is < 5% of the solar Si abundance).

The first detection of the silicate *absorption* feature in AGNs was made at 9.7 μm for the prototypical Seyfert 2 galaxy NGC 1068 (Rieke & Low 1975; Kleinmann et al. 1976), indicating the presence of a large column of silicate dust in the line-of-sight to the nucleus. It is known now that most of the type 2 AGNs display silicate *absorption* bands (e.g. see Roche et al. 1991, Siebenmorgen et al. 2004) as expected – for a centrally heated optically thick torus viewed edge-on,

the silicate features should be in absorption. Spatially resolved mid-IR spectra obtained for NGC 1068 (Mason et al. 2006, Rhee & Larkin 2006) and Circinus (Roche et al. 2006) have revealed striking variations in continuum slope, silicate feature profile and depth.

However, it appears that the $9.7\ \mu\text{m}$ silicate absorption profile of AGNs differs from that of the Milky Way. Jaffe et al. (2004) found that the $9.7\ \mu\text{m}$ silicate absorption spectrum of NGC 1068 shows a relatively flat profile from 8 to $9\ \mu\text{m}$ and then a sharp drop between 9 and $10\ \mu\text{m}$; in comparison, the Galactic silicate absorption profiles begin to drop already at $\sim 8\ \mu\text{m}$. They obtained a much better fit to the $9.7\ \mu\text{m}$ absorption feature of NGC 1068 by using the profile of calcium aluminium silicate $\text{Ca}_2\text{Al}_2\text{SiO}_7$, a high-temperature dust species found in some supergiant stars (Speck et al. 2000). It would be interesting to know if the amount of calcium required to account for the observed absorption is consistent with abundance constraints. Very recently, Roche et al. (2007) reported the detection of a spectral structure near $11.2\ \mu\text{m}$ in NGC 3094, indicative of the possible presence of crystalline silicates in AGNs.

For type 1 AGNs viewed face-on, one would expect to see the silicate features in *emission* since the silicate dust in the surface of the inner torus wall will be heated to temperatures of several hundred kelvin by the radiation from the central engine, allowing for a direct detection of the $9.7\ \mu\text{m}$ and $18\ \mu\text{m}$ silicate bands emitted from this hot dust. However, their detection (using *Spitzer*) has only very recently been reported in a number of type 1 AGNs (Hao et al. 2005, Siebenmorgen et al. 2005, Sturm et al. 2005, Weedman et al. 2005, Shi et al. 2006). Siebenmorgen et al. (2005) postulated that the AGN luminosity determines whether the silicate emission bands are prominent or not (i.e., they may be present only in the most luminous AGNs), but this idea was challenged by their detection in the low-luminosity AGN NGC 3998, a type 1 LINER galaxy (Sturm et al. 2005).

The $9.7\ \mu\text{m}$ silicate emission profiles of both quasars (high luminosity counterparts of Seyfert 1 galaxies; Hao et al. 2005, Siebenmorgen et al. 2005) and the low-luminosity AGN NGC 3998 (Sturm et al. 2005) peak at a much longer wavelength ($\sim 11\ \mu\text{m}$), inconsistent with “standard” silicate ISM dust (which peaks at $\sim 9.7\ \mu\text{m}$). The $9.7\ \mu\text{m}$ feature of NGC 3998 is also much broader than that of the Galactic ISM (Sturm et al. 2005). The deviations of the silicate emission profiles of type 1 AGNs from that of the Galactic ISM dust may indicate differences in the dust composition, grain size distribution, or radiative transfer effects (Sturm et al. 2005, Levenson et al. 2007). The red tail of the $18\ \mu\text{m}$ silicate feature of NGC 3998 is significantly weaker than that of the bright quasars (Sturm et al. 2005), suggesting that there may exist significant environmental variations. Finally, it is worth noting that the $9.7\ \mu\text{m}$ silicate feature of Mkn 231, a peculiar type 1 Seyfert galaxy, is also seen in *absorption* peaking at $\sim 10.5\ \mu\text{m}$ (Roche et al. 1983).

3.4. The 3.3, 6.2, 7.7, 8.6 and $11.3\ \mu\text{m}$ PAH Emission Features

The distinctive set of “Unidentified Infrared” (UIR) emission features at 3.3, 6.2, 7.7, 8.6, and $11.3\ \mu\text{m}$, now generally identified as the vibrational modes of PAH molecules (Léger & Puget 1984; Allamandola et al. 1985), are seen in a wide variety of Galactic and extragalactic regions (see Draine & Li 2007). In the Milky Way diffuse interstellar medium (ISM), PAHs, containing ~ 45 ppm (parts

per million, relative to H) C, account for $\sim 20\%$ of the total power emitted by interstellar dust (Li & Draine 2001b). The *ISO* (Infrared Space Observatories) and *Spitzer* imaging and spectroscopy have revealed that PAHs are also a ubiquitous feature of external galaxies. Recent discoveries include the detection of PAH emission in a wide range of systems: distant Luminous Infrared Galaxies (LIRGs) with redshift z ranging from 0.1 to 1.2 (Elbaz et al. 2005), distant Ultraluminous Infrared Galaxies (ULIRGs) with redshift $z \sim 2$ (Yan et al. 2005), distant luminous submillimeter galaxies at redshift $z \sim 2.8$ (Lutz et al. 2005), elliptical galaxies with a hostile environment (containing hot gas of temperature $\sim 10^7$ K) where PAHs can be easily destroyed through sputtering by plasma ions (Kaneda et al. 2005), faint tidal dwarf galaxies with metallicity $\sim Z_{\odot}/3$ (Higdon et al. 2006), and galaxy halos (Irwin & Madden 2006, Engelbracht et al. 2006).

However, the PAH features are absent in AGNs, as first noticed by Roche et al. (1991). This is commonly interpreted as the destruction of PAHs by extreme UV and soft X-ray photons in AGNs (Roche et al. 1991; Voit 1991, 1992; Siebenmorgen et al. 2004). Genzel et al. (1998) proposed to use the line-to-continuum ratio of the $7.7 \mu\text{m}$ PAH feature as a discriminator between starburst and AGN activity in ULIRGs (i.e. whether the dominant luminosity source of ULIRGs is an AGN or a starburst). We should note that the PAH emission features are detected in some Seyfert 2 galaxies, but they are from the circumnuclear star-forming regions, not from the AGNs (e.g. see Le Floc'h et al. 2001, Siebenmorgen et al. 2004).

3.5. The Ice Absorption Features

Grains in dark molecular clouds (usually with $A_V > 3$ mag) obtain ice mantles consisting of H_2O , NH_3 , CO , CH_3OH , CO_2 , CH_4 , H_2CO and other molecules (with H_2O as the dominant species), as revealed by the detection of various ice absorption features (e.g., H_2O : $3.1, 6.0 \mu\text{m}$; CO : $4.67 \mu\text{m}$; CO_2 : $4.27, 15.2 \mu\text{m}$; CH_3OH : $3.54, 9.75 \mu\text{m}$; NH_3 : $2.97 \mu\text{m}$; CH_4 : $7.68 \mu\text{m}$; H_2CO : $5.81 \mu\text{m}$; XCN^- : $4.62 \mu\text{m}$). The ice absorption features are also seen in most ULIRGs (e.g. see Spoon et al. 2002), indicating the presence of a large quantity of molecular material in ULIRGs. However, the ice absorption features are not expected in AGNs due to the high dust temperatures (because of the immense bolometric luminosity emitted from the AGN) – the dust in the torus, even at a distance of ~ 100 pc, is too warm (> 100 K) for ice mantles to survive.

4. IR Emission Modeling – Inferring Dust Size and Torus Geometry?

To constrain the dust size distribution and the size and geometry of the dust torus, various models have been proposed to explain the observed IR emission spectral energy distribution (SED) of AGNs, radiated by the circumnuclear dust heated by the AGN illumination. These models assume a wide range of torus geometries: uniform density annular (cylindrical) rings of a few pc with an extremely large optical depth $\tau_{\text{UV}} > 1000$ (Pier & Krolik 1992, 1993), optically thick plane parallel slabs of a few thousand pc (Laor & Draine 1993), extended tori of hundreds of pc (Granato & Danese 1994, Granato et al. 1997), geometrically thin, optically thick spherical shells (Rowan-Robinson 1995), tapered disks (Efstathiou & Rowan-Robinson 1995, Stenholm 1995), optically thick, flared disks (Manske et al. 1998), clumpy tori (Nenkova et al. 2002), and other more complicated torus geometries (van Bemmell & Dullemond 2003, Schartmann et

al. 2005). In order to suppress the $9.7\ \mu\text{m}$ silicate emission feature (which was not detected until very recently by *Spitzer*; see §3.3), some models hypothesized that the dust in AGNs must be large ($a < 10\ \mu\text{m}$) or small silicate grains must be depleted (e.g. see Laor & Draine 1993, Granato & Danese 1994). Some models ascribed the suppression of the $9.7\ \mu\text{m}$ silicate emission feature to clumpiness (Nenkova et al. 2002) or the strong anisotropy of the source radiation (Manske et al. 1998). Apparently, more modeling efforts are required to account for the very recent detection of the $9.7\ \mu\text{m}$ and $18\ \mu\text{m}$ silicate emission features in type 1 AGNs and the recent high resolution IR imaging observations which seem to show that the torus size is no more than a few parsecs (see Elitzur 2006 and references therein). It is well known that the SED modeling alone does not uniquely determine the dust size distribution and the dust spatial distribution.

Acknowledgments. I thank L.C. Ho and J.M. Wang for inviting me to attend this stimulating conference. I also thank B. Czerny, C.M. Gaskell, S.L. Liang, R. Maiolino, and C. Willott for their comments and/or help in preparing for this article. Partial support by NASA/Spitzer theory programs and the University of Missouri Research Board is gratefully acknowledged.

References

- Adamson, A.J., et al. 1999, ApJ, 512, 224
 Allamandola, L.J., Tielens, A.G.G.M., & Barker, J.R. 1985, ApJ, 290, L25
 Antonucci, R.R.J. 1993, ARA&A, 31, 473
 Baker, J.C., & Hunstead, R.W. 1995, ApJ, 452, L95
 Barvainis, R. 1987, ApJ, 320, 537
 Buchanan, C.L., et al., 2006, AJ, 132, 401
 Chiar, J.E., et al. 2006, ApJ, 651, 268
 Cardelli, J.A., Clayton, G.C., & Mathis, J.S. 1989, ApJ, 345, 245
 Crenshaw, D.M., Kraemer, S.B., Bruhweiler, F.C., & Ruiz, J.R. 2001, ApJ, 555, 633
 Crenshaw, D.M., et al. 2002, ApJ, 566, 187
 Czerny, B., Li, J., Loska, Z., & Szczerba, R. 2004, MNRAS, 348, 54
 Draine, B.T., & Li, A. 2001, ApJ, 551, 807
 Draine, B.T., & Li, A. 2007, ApJ, 657, 810
 Efstathiou, A., & Rowan-Robinson, M. 1995, MNRAS, 273, 649
 Elbaz, D., Le Floc'h, E., Dole, H., & Marcillac, D. 2005, A&A, 434, L1
 Elitzur, M. 2006, New Astronomy Review, 50, 728
 Engelbracht, C.W., et al. 2006, ApJ, 642, L127
 Francis, P.J., et al. 1991, ApJ, 373, 465
 Gaskell, C.M., et al. 2004, ApJ, 616, 147
 Gaskell, C.M., & Benker, A.J. 2007, ApJ, in press
 Genzel, R., et al. 1998, ApJ, 498, 579
 Granato, G.L., & Danese, L. 1994, MNRAS, 268, 235
 Granato, G.L., Danese, L., & Franceschini, A. 1997, ApJ, 486, 147
 Greenberg, J.M., Li, A., et al. 1995, ApJ, 455, L177
 Hao, L., et al. 2005, ApJ, 625, L75
 Heisler, C.A., Lumsden, S.L., & Bailey, J.A. 1997, Nature, 385, 700
 Higdon, S.J., Higdon, J.L., & Marshall, J. 2006, ApJ, 640, 768
 Ho, L.C. 1999, Adv. Space Res., 23, 813
 Hopkins, P.F., et al. 2004, AJ, 128, 1112
 Imanishi, M., et al. 1997, PASJ, 49, 69
 Irwin, J.A., & Madden, S.C. 2006, A&A, 445, 123
 Joblin, C., Léger, A., & Martin, P. 1992, ApJ, 393, L79
 Jones, A.P., Duley, W.W., & Williams, D.A. 1990, QJRAS, 31, 567
 Kaneda, H., Onaka, T., & Sakon, I. 2005, ApJ, 632, L83

- Kleinmann, D.E., Gillett, F.C., & Wright, E.L. 1976, *ApJ*, 208, 42
Koornneef, J., & Code, A.D. 1981, *ApJ*, 247, 860
Laor, A., & Draine, B.T. 1993, *ApJ*, 402, 441
Le Floch, E., et al. 2001, *A&A*, 367, 487
Léger, A., & Puget, J. L. 1984, *A&A*, 137, L5
Lequeux, J., et al. 1982, *A&A*, 113, L15
Levenson, N.A., et al. 2007, *ApJ*, 654, L45
Li, A., & Draine, B.T. 2001a, *ApJ*, 550, L213
Li, A., & Draine, B.T. 2001b, *ApJ*, 554, 778
Li, A., & Greenberg, J.M. 1997, *A&A*, 323, 566
Li, A., & Greenberg, J.M. 2002, *ApJ*, 577, 789
Lutz, D., et al. 2005, *ApJ*, 625, L83
Maiolino, R., Marconi, A., & Oliva, E. 2001a, *A&A*, 365, 37
Maiolino, R., et al. 2001b, *A&A*, 365, 28
Manske, V., Henning, Th., & Men'shchikov, A.B. 1998, *A&A*, 331, 52
Mason, R.E., Wright, G.S., Pendleton, Y.J., & Adamson, A. 2004, *ApJ*, 613, 770
Mason, R.E., et al. 2006, *ApJ*, 640, 612
Mason, R.E., Wright, G.S., Adamson, A., & Pendleton, Y.J. 2007, *ApJ*, 656, 798
Mennella, V., Brucato, J.R., Colangeli, L., & Palumbo, P. 1999, *ApJ*, 524, L71
Nandy, K., et al. 1981, *MNRAS*, 196, 955
Nenkova, M., Ivezić, Z., & Elitzur, M. 2002, *ApJ*, 570, L9
Osterbrock, D.E., & Ferland, G.J. 2006, *Astrophysics of Gaseous Nebulae and Active Galactic Nuclei*, 2nd ed, University Science Books
Pendleton, Y.J., & Allamandola, L.J. 2002, *ApJS*, 138, 75
Pier, E.A., & Krolik, J.H. 1992, *ApJ*, 401, 99; 1993, *ApJ*, 418, 673
Prévot, M.L., et al. 1984, *A&A*, 132, 389
Rhee, J.H., & Larkin, J.E. 2006, *ApJ*, 640, 625
Richards, G.T., et al. 2003, *AJ*, 126, 1131
Rieke, G.H., & Low, F.J. 1975, *ApJ*, 199, L13
Roche, P.F., Aitken, D.K., & Whitmore, B. 1983, *MNRAS*, 205, P21
Roche, P.F., Aitken, D.K., & Smith, C.H. 1991, *MNRAS*, 252, 282
Roche, P.F., et al. 2006, *MNRAS*, 367, 1689
Roche, P.F., Packham, C., Aitken, D.K., & Mason, R.E. 2007, *MNRAS*, 375, 99
Rodríguez-Ardila, A., & Mazzalay, X. 2006, *MNRAS*, 367, L57
Rowan-Robinson, M. 1995, *MNRAS*, 272, 737
Schartmann, M., et al. 2005, *A&A*, 437, 861
Shi, Y., et al. 2006, *ApJ*, 653, 127
Siebenmorgen, R., Krügel, E., & Spoon, H.W.W. 2004, *A&A*, 414, 123
Siebenmorgen, R., Haas, M., Krügel, E., & Schulz, B. 2005, *A&A*, 436, L5
Shang, Z., et al. 2005, *ApJ*, 619, 41
Speck, A.K., Barlow, M.J., Sylvester, R.J., & Hofmeister, A.M. 2000, *A&AS*, 146, 437
Spoon, H.W.W., et al. 2002, *A&A*, 385, 1022
Stecher, T.P. 1965, *ApJ*, 142, 1683
Stenholm, L. 1995, *A&A*, 290, 393
Sturm, E., et al. 2005, *ApJ*, 629, L21
Tran, H.D. 2003, *ApJ*, 583, 632
Urry, C.M., & Padovani, P. 1995, *PASP*, 107, 803
van Bemmell, I.M., & Dullemond, C.P. 2003, *A&A*, 404, 1
Voit, G.M. 1991, *ApJ*, 379, 122; 1992, *MNRAS*, 258, 841
Weedman, D.W., et al. 2005, *ApJ*, 633, 706
Weingartner, J.C., & Murray, N. 2002, *ApJ*, 580, 88
Willott, C.J. 2005, *ApJ*, 627, L101
Wright, G.S., Bridger, A., Geballe, T.R., & Pendleton, Y. 1996, in *New Extragalactic Perspectives in the New South Africa*, 143
Yan, L., et al. 2005, *ApJ*, 628, 604